QED cascades induced by circularly polarized laser fields

N. V. Elkina,[1] A. M. Fedotov,[2] I. Yu. Kostyukov,[3] M. V. Legkov,[2] N. B. Narozhny,[2] E. N. Nerush,[3] and H. Ruhl[1]

[1]*Ludwig-Maximilians Universität München, 80539, Germany*
[2]*National Research Nuclear University MEPhI, Moscow, 115409, Russia*
[3]*Institute of Applied Physics, Russian Academy of Sciences, 603950, Nizhny Novgorod, Russia*

(Received 22 October 2010; published 12 May 2011)

The results of Monte-Carlo simulations of electron-positron-photon cascades initiated by slow electrons in circularly polarized fields of ultrahigh strength are presented and discussed. Our results confirm previous qualitative estimations [A. M. Fedotov *et al.*, Phys. Rev. Lett. **105**, 080402 (2010)] of the formation of cascades. This sort of cascade has revealed a new property of restoration of energy and dynamical quantum parameter due to acceleration of electrons and positrons by the field. This may become a dominating feature of laser-matter interactions at ultrahigh intensities. Our approach incorporates radiation friction acting on individual electrons and positrons.

DOI: 10.1103/PhysRevSTAB.14.054401 PACS numbers: 52.27.Ep, 52.50.Dg, 41.75.Jv, 42.50.Ct

I. INTRODUCTION

The dramatic progress in laser technology has enabled a novel area of studies exploring laser-matter interactions at ultrahigh intensity [1]. The intensity level of 2×10^{22} W/cm^2 has recently been achieved [2] and two projects [3,4] aiming at intensity levels up to 10^{26} W/cm^2 are under way. Furthermore, several proposals [5–7] have been put forward, which reach even higher intensities. One of the key phenomena of laser-matter interactions at ultrahigh intensities of our interest is the occurrence of QED cascades [4,8–10]. These cascades (also called avalanches, or showers) are caused by successive events of hard photon emissions and electron-positron pair photoproduction by hard photons. As predicted in Ref. [10] on the basis of qualitative estimations, the cascades may arise as soon as the laser field strength exceeds the threshold value of $E_* = \alpha E_S$, where $\alpha = e^2/\hbar c \approx 1/137$ is the fine structure constant and $E_S = m^2c^3/e\hbar = 1.32 \times 10^{16}$ V/cm is the characteristic QED field. Such a field strength corresponds to the intensity of $\sim 10^{25}$ W/cm^2.

Previously QED cascades have been observed and studied as a part of extensive air showers (EAS) in the context of the passage through the atmosphere [11–13] of ultrahigh energy particles that originate from cosmic rays. However, similar processes can be observed in the external electromagnetic field as well. In this case bremsstrahlung is replaced by the nonlinear Compton scattering and the Bethe-Heitler process is replaced by the nonlinear Breit-Wheeler process. The latter processes are well studied both theoretically [14–19] and in laser experiments [20] and are probably of great importance for astrophysics (see, e.g., [21]).

An important novel distinctive feature of the cascades in the ultrastrong laser field, compared to situations ever studied previously, is that the laser field is not only able to be a target for ultrarelativistic electrons and hard photons, but can also accelerate the charged particles to ultrarelativistic energies.

As a result, the cascades can be produced even by initially slow electrons or positrons, if they were somehow injected into the strong field region. Moreover, the mean energy of the particles is no longer decreasing in the course of the cascade development due to its redistribution among the permanently growing number of the created particles. Instead, the mean energy is being restored at the expense of the energy extracted from the laser field. This must lead to a vast increase of the cascade yield, as compared to the cascades in media or in strong magnetic fields. In this case the cascade multiplicity would be restricted either by the dwell time of the particles in the focal region of the laser field, or even (under more extreme conditions) by the total energy stored in the laser field. In the latter case the focused laser pulses would be depleted by cascade production.

As it will be explained in more detail below, the restoration mechanism works if the particles can be accelerated transversely to the field. Several authors [8,10] conjectured that this may be indeed the case on the basis of qualitative analysis for the model of uniformly rotating electric fields.

In the EAS theory, the 1D approximation is often used because spreading in the transverse direction is inessential for ultrarelativistic particles and has no significance for that problem. Besides, the cascade equations can be solved in this case analytically within the ultrarelativistic approximation by means of the Mellin transform [12,13]. The results of such analytic theory are in good agreement with both experiments [11,12] and Monte-Carlo simulations [22]. The attempts to treat the cascades in strong magnetic fields on similar grounds are also known [23]. However, although the 1D approximation remains valid, the cascade equations cannot be simplified using the Mellin transform unless some further approximation is made. According to Monte-Carlo simulations [24], the resulting analytical approach works much worse here than in the case of 1D approximation for EAS. In our case of cascades arising in a laser field, the structure of the cascade equations (see the Appendix) is the same as for the magnetic field, but it is impossible to incorporate restoration mechanism within the 1D approximation in momentum space. This means that our problem is essentially two or three dimensional.

In this work we report on the first results of the Monte-Carlo simulations of cascades produced by initially slow electrons in a uniformly rotating homogeneous electric field. Such a field can be obtained practically at the antinodes of a standing electromagnetic wave. The choice of the field model is uniquely specified by the existence of reasonable qualitative estimations for scaling of the basic cascade characteristics for this particular case [10]. Our goal was to prove explicitly the existence of the restoration mechanism and to test the estimations [10] by direct numerical simulations.

The paper is organized as follows. In Sec. II, which can be considered as a technical introduction, we review and collect the known information on the elementary quantum processes: single photon emission by electrons and pair creation by hard photons in strong fields of arbitrary configuration. Though this information is not completely new, it is of essential importance for our presentation and is spread among the literature on the subject. After that, in Sec. III we present the reasoning in favor of the energy restoration mechanism for cascades in electromagnetic fields. In Sec. IV we formulate the assumptions of our model, present the details of our Monte-Carlo routine, and discuss the results obtained by numerical simulations. These results are compared to the known estimations. Summary and discussion is given in Sec. V. Finally, in the Appendix, we discuss the cascade equations for our problem and explicitly demonstrate that, contrary to the recent doubts [25], the approach we use takes proper account of radiation friction for ultrarelativistic electrons.

II. QUANTUM PROCESSES WITH HIGH-ENERGY PARTICLES IN A STRONG ELECTROMAGNETIC FIELD

General properties of radiation of ultrarelativistic particles are well known [26]. The momenta of the products of any decay of an ultrarelativistic particle are directed mainly in the forward direction along the momentum $\boldsymbol{p}$ of the particle: they are contained almost entirely within the small range of angles $\Delta\theta \sim \gamma^{-1}$ around the direction of $\boldsymbol{p}$. Here $\gamma = \varepsilon/mc^2$ is the Lorentz factor, and ε is the energy of the particle. Thus, radiation of a charged ultrarelativistic particle is visible at the point of observation only for a short period of time $\tau \sim mc/eF_\perp$ during which its momentum rotates through the angle of the order $\Delta\theta$. Here, $F_\perp$ denotes the transverse (to the direction of motion) component of the field.

The decay processes in external electromagnetic fields are ruled, see, e.g., [27], by the Lorentz and gauge invariant parameter

$$\chi = \frac{e\hbar}{m^3c^4}\sqrt{\left(\frac{\varepsilon \boldsymbol{E}}{c} + \boldsymbol{p}\times\boldsymbol{H}\right)^2 - (\boldsymbol{p}\cdot\boldsymbol{E})^2}, \tag{1}$$

which, in particular, determines whether the process is controlled by classical or quantum electrodynamics. If $\chi \ll 1$, the loss of the energy by an electron due to emission of a photon is inessential and radiation can be treated classically, whereas at $\chi \gtrsim 1$ such emission causes both a loss of the electron energy and longitudinal recoil deflecting the electron trajectory. In the latter case the radiation should be considered in the framework of QED.

In what follows, we assume that $E, H \ll E_S$. On the other hand, we assume that the field is of relativistic strength in the sense that the dimensionless field amplitude $a_0 = e\sqrt{-A_\mu A^\mu}/(mc) \gg 1$, where A_μ is the 4-vector of the field potential. The characteristic time of the field variation essentially exceeds τ under this condition. Thus, the field can be considered constant with respect to the decay processes. If, in addition, $\chi \gg E/E_S$, then *any* field looks as a constant crossed field [27] and we can apply the theory of quantum processes in such a field which was given in Refs. [15,19,27].

According to this theory, the energy distribution of the probability rate for photon emission by ultrarelativistic electrons in an electromagnetic field is given by

$$\frac{dW_{\rm rad}(\varepsilon_\gamma)}{d\varepsilon_\gamma} = -\frac{\alpha m^2c^4}{\hbar\varepsilon_e^2}\left\{\int_x^\infty {\rm Ai}(\xi)d\xi + \left(\frac{2}{x} + \chi_\gamma\sqrt{x}\right){\rm Ai}'(x)\right\}, \tag{2}$$

where $x = (\chi_\gamma/\chi_e\chi_e')^{2/3}$, ${\rm Ai}(x) = (1/\pi)\int_0^\infty \cos(\xi^3/3 + \xi x)d\xi$ is the Airy function, ε_γ and ε_e are the energies of the emitted photon and the initial electron, respectively. χ_e, $\chi_e' = \chi_e - \chi_\gamma$ and χ_γ $(0 < \chi_\gamma < \chi_e)$ are the dimensionless quantum parameters for the electron before and after emission, and for the emitted photon, respectively.

Note that the probability rate (2) displays singular behavior at $\varepsilon_\gamma \to 0$, $dW_{\rm rad}(\varepsilon_\gamma)/d\varepsilon_\gamma = O(\varepsilon_\gamma^{-2/3})$. However, in the adopted approximation this singularity is weaker than the usual $O(\varepsilon_\gamma^{-1})$ infrared divergence of perturbative QED [27,28]. As a result, the total radiation probability rate is convergent. In general, the sector of small photon frequencies is not important in the domain of parameters considered in this paper, since the average frequency of the emitted radiation exceeds the frequency of the driving field essentially.

The energy distribution of the probability rate for direct pair creation by hard photons ($\varepsilon_\gamma \gg mc^2$) is given by

$$\frac{dW_{\rm cr}(\varepsilon_e)}{d\varepsilon_e} = \frac{\alpha m^2 c^4}{\hbar \varepsilon_\gamma^2}\left\{\int_x^\infty \mathrm{Ai}(\xi)d\xi + \left(\frac{2}{x} - \chi_\gamma\sqrt{x}\right)\mathrm{Ai}'(x)\right\}, \tag{3}$$

where the indices "γ" and "e" refer this time to the initial photon and to the created electron, respectively. For the created positron, we have $\chi_e' = \chi_\gamma - \chi_e$ $(0 < \chi_e < \chi_\gamma)$. Formula (3) is completely symmetric with respect to electrons and positrons, remaining unchanged under the replacement $\chi_e \leftrightarrow \chi_e'$. The similarity between formulas (2) and (3) is explained by the fact that these two processes are two cross channels of the same reaction [27].

The total probability rates for both processes cannot be written in terms of known special functions and should be obtained by numerical integrations. However, they allow simple asymptotic expressions in the limit of large χ_e and χ_γ, respectively. We have

$$W_{\rm rad} \approx 1.46\frac{\alpha m^2 c^4}{\hbar \varepsilon_e}\chi_e^{2/3}, \qquad \chi_e \gg 1, \tag{4}$$

and

$$W_{\rm cr} \approx 0.38\frac{\alpha m^2 c^4}{\hbar \varepsilon_\gamma}\chi_\gamma^{2/3}, \qquad \chi_\gamma \gg 1. \tag{5}$$

For small values of the quantum parameter χ_γ, the probability rate for pair photoproduction $W_{\rm cr}$ is suppressed exponentially. This corresponds to the impossibility of pair creation in the classical limit.

Equation (2) determines the energy distribution function for the photons emitted by an electron with the momentum $\boldsymbol{p}_e$ and the energy ε_e. If $\gamma_e \gg 1$, the momentum of this photon is given by $\boldsymbol{p}_\gamma = (\varepsilon_\gamma/p_e)\boldsymbol{p}_e$. The energy and the momentum of the recoil electron should be determined from the conservation laws. In the electromagnetic background, they are of the form $p_e^\mu + q^\mu = p_e'^\mu + p_\gamma^\mu$, where q^μ is the 4-momentum extracted from the field. However, for ultrarelativistic particles we can write $\boldsymbol{p}_e' = \boldsymbol{p}_e - \boldsymbol{p}_\gamma$. This is because $q \lesssim eF\tau \lesssim mc \ll p_e, p_e', p_\gamma$ within the accuracy of our approximation. The same argument can be applied to the process of pair creation by hard photons as well.

In addition to one-photon emission and direct pair photoproduction reviewed above, there exist more complicated higher-order processes, such as, e.g., the two-photon emission $e^- \to e^-\gamma\gamma$ or the trident process $e^- \to e^-e^-e^+$. Their specific feature is that the intermediate particle is off the mass shell, i.e., is virtual. However, in strong field cases of our interest the two-step processes dominate [8,9,20]. For this reason, we do not consider higher-order processes in the sequel.

III. BASIC ESTIMATES FOR CASCADE PRODUCTION IN A ROTATING ELECTRIC FIELD

Since there is no difference whether an electron or a positron initiates a cascade, we assume in this section that our cascade is initiated by a positron ($e > 0$).

Consider a positron in a homogeneous, uniformly rotating electric field

$$\boldsymbol{E}(t) = \{E_0\cos\omega t, E_0\sin\omega t\}. \tag{6}$$

The equation of motion

$$\dot{\boldsymbol{p}}(t) = e\boldsymbol{E}(t), \tag{7}$$

with the initial condition $\boldsymbol{p}(t_0) = \boldsymbol{p}_0$, can be easily solved:

$$\begin{aligned} p_x(t) &= p_{0x} + mca_0(\sin\omega t - \sin\omega t_0),\\ p_y(t) &= p_{y0} - mca_0(\cos\omega t - \cos\omega t_0). \end{aligned} \tag{8}$$

Here, $a_0 = eE_0/m\omega c$ is the dimensionless field amplitude.

Let us assume first that the positron is at rest ($\boldsymbol{p}_0 = 0$) initially ($t_0 = 0$). Equations (6) and (8) show that the energy and the quantum parameter χ of the positron for this case depend on time as

$$\varepsilon_e(t) = mc^2\sqrt{1 + 4a_0^2\sin^2\frac{\omega t}{2}}, \tag{9a}$$

$$\chi_e(t) = \frac{e\hbar E_0}{m^2c^3}\sqrt{1 + 4a_0^2\sin^4\frac{\omega t}{2}}. \tag{9b}$$

Both quantities are increasing initially. They are oscillating with the period $2\pi/\omega$ of the rotation of the field. The amplitudes of these oscillations, $\varepsilon_m \approx 2mc^2a_0$, $\chi_m \approx 2a_0(E_0/E_S) = 2(\hbar\omega/mc^2)a_0^2$ are proportional to a_0 and a_0^2, respectively, and are quite large under our basic assumptions. For example, χ_m approaches unity already at $a_0 \sim a_{0c} = 500$ for an optical rotation frequency, $\hbar\omega = 1$ eV. This corresponds to the field strength $E_0 \sim 10^{-3}E_S \sim 10^{13}$ V/cm and intensity 10^{24} W/cm^2. Since $\chi_m \sim 1$ under such conditions, the positron, according to the preceding section, is able to emit a hard photon with $\chi_\gamma \sim \chi_e \sim 1$, which, in turn, can create an electron-positron pair. However, at such intensities a new generation of pairs is typically produced on the time scale π/ω, and the whole pair generation process may be rather sensitive to peculiarities of the field model. As we will discuss below, stable cascade formation is expected at higher intensity levels.

The formulas (9a) and (9b) become especially simple for stronger fields $a_0 \gg a_{0c}$, because in this case the value $\chi_e \sim 1$ is reached within just a small fraction $t_{\rm acc}$ of the rotation period. We have

$$\varepsilon_e(t) \approx eE_0ct, \qquad \frac{1}{\omega a_0} \ll t \ll \frac{1}{\omega}, \tag{10a}$$

$$\chi_e(t) \approx \frac{1}{2}\left(\frac{E_0}{E_S}\right)^2\frac{mc^2\omega}{\hbar}t^2, \qquad \frac{1}{\omega\sqrt{a_0}} \ll t \ll \frac{1}{\omega}. \tag{10b}$$

Equation (10a) immediately follows from the fact that the positron is initially accelerating almost along the field. Let us note now that according to Eqs. (6) and (8) the momentum of the positron in the case $\boldsymbol{p}(0) = 0$ constitutes the angle with both the instant direction of the field and the x axis exactly equal to $\omega t/2$. This is because the particle does not follow the rotation of the field precisely due to its inertia. As a consequence, the transverse (to the momentum of the particle) component of the field increases as $E_\perp = E_0 \sin(\omega t/2) \approx E_0 \omega t/2$. Since $\chi_e(t) \approx E_\perp \gamma / E_S$, we arrive immediately at Eq. (10b). The similar behavior of the energy and the parameter χ with time has been observed in Ref. [10] for generic field configurations.

As it follows from Eq. (10b), the quantum parameter χ_e becomes of the order of unity over the period of time $t_{\rm acc}$,

$$t_{\rm acc} \sim \frac{\hbar}{\alpha m c^2 \mu} \sqrt{\frac{mc^2}{\hbar\omega}}. \tag{11}$$

Here we have introduced a new dimensionless field intensity parameter $\mu = E/E_*$, $E_* = \alpha E_S \approx E_S/137$, which is appropriate for the cascade problem [10]. The parameter μ is related to the commonly accepted parameter a_0 by $\mu = (\hbar\omega/\alpha m c^2) a_0$. According to Ref. [10], the cascades can be caused by initially slow particles if $\mu \gtrsim 1$.

In the course of hard photon emission, the value of the quantum parameter χ_e is shared between the positron and the emitted photon [29], $\chi_e \approx \chi_\gamma + \chi_e'$. If $\chi_e \gtrsim 1$ then both χ_γ and χ_e' are less than χ_e but are of comparable values $\chi_e' \sim \chi_\gamma \lesssim \chi_e$. Although propagation of the resulting hard photon is not affected by the field, nevertheless its χ_γ continues to increase after emission just due to rotation of the field.

In order to understand better what is happening at the successive stages of cascade development, let us return to Eq. (8) and consider the general initial conditions. In the case $\boldsymbol{H} = 0$ the sign of the time derivative of (1) is completely determined by the sign of the quantity $-(\boldsymbol{p}\cdot\boldsymbol{E}) \times (\boldsymbol{p}\cdot\dot{\boldsymbol{E}})$. The zones in the $\boldsymbol{p}_0$ plane where $\dot{\chi}_e$ is positive for a parental positron at the moment of photon emission $t = t_0$ are shaded in Fig. 1. Since the secondary particles are created with momenta parallel to the momentum of the parental particle, their momenta also lie in the shaded sector and hence the parameter χ of the recoil positron is also growing. The same will be true for successive pair creation processes as well. The momenta of created electron and positron also lie in the sector with $\dot{\chi} > 0$ and their transverse (to the momentum of the parental photon) momenta are both growing in magnitude being oppositely directed.

The fact that the field repeatedly restores the values of parameter χ of the particles which decrease at every event of photon emission plays the key role for cascade development. The preceding paragraph explains the restoration mechanism for the case of a homogenous uniformly rotating electric field in detail.

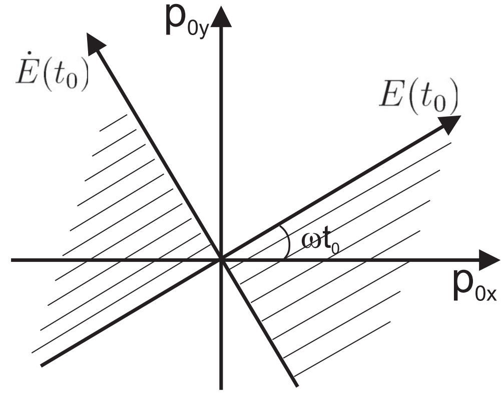

FIG. 1. The sign of $\dot{\chi}_e(t)$ along the particle trajectory at $t = t_0$ in different zones of the $p_{0x}p_{0y}$ plane. The shaded zones correspond to acceleration (increase of χ_e) of positrons and electrons.

Though the spatial picture of the cascade development is very complicated (see Fig. 2), one can obtain some general estimates in the high-field limit $\mu \gg 1$ [10]. Basing on the similarity of the probability rates (4) and (5), as well as time dependencies of the angles between the momenta and the field strength for all particles (positrons, electrons, and photons), we will not distinguish between these three sorts

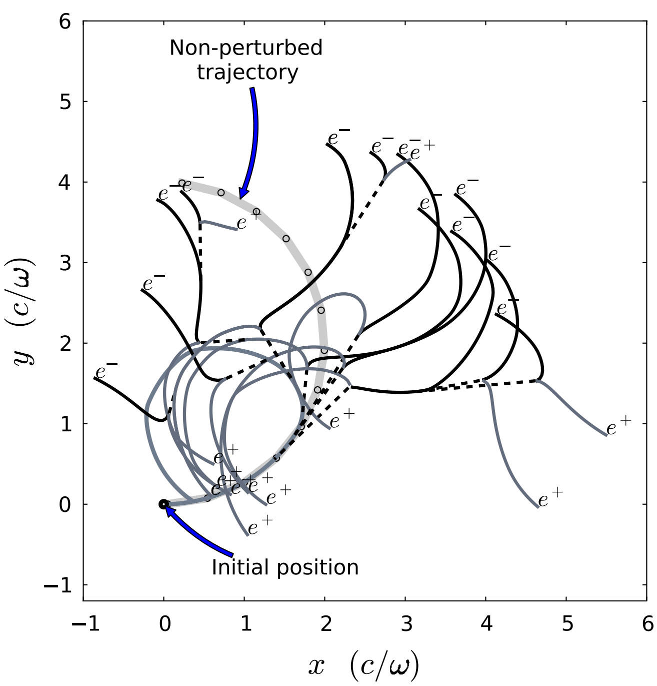

FIG. 2. Spatial picture of the formation of the cascade initiated by a positron in the homogeneous uniformly rotating electric field (obtained by a Monte-Carlo simulation with $a_0 = 2 \times 10^3$ and $\hbar\omega = 1$ eV). Legend: Trajectories of electrons and positrons are shown as black and gray curves, respectively. The hard photons which have created pairs during the simulation time are shown as the dashed lines. The trajectory of the primary positron ignoring any QED processes is plotted as the thick light gray curve.

of particles and use the model of a simple doubling chain process. Such a model must give a correct order-of-magnitude estimate.

Let us denote by t_e the typical lifetime for electrons and positrons with respect to hard photon emission. The same quantity defines the lifetime of photons with respect to pair creation up to an order of magnitude. The lifetime t_e, the typical energy ε and the quantum parameter χ of the particles, as well as the angle between their momenta and the field strength θ can be estimated as [10]

$$t_e \sim \frac{\hbar}{\alpha mc^2 \mu^{1/4}} \sqrt{\frac{mc^2}{\hbar\omega}}, \tag{12a}$$

$$\varepsilon_{\rm est} \sim mc^2 \mu^{3/4} \sqrt{\frac{mc^2}{\hbar\omega}}, \qquad \chi_{\rm est} \sim \mu^{3/2}, \tag{12b}$$

$$\theta_{\rm est} \sim \omega t_e \sim \frac{1}{\alpha \mu^{1/4}} \sqrt{\frac{\hbar\omega}{mc^2}}. \tag{12c}$$

Under the condition $\mu \gg 1$, as is assumed here, we have $\theta \ll 1$ and $\chi \gg 1$. The latter inequality approves the choice of the asymptotic expressions (4) and (5). In addition, we have the following hierarchy of the time scales $t_{\rm acc} \ll t_e$, which assures that exactly hard photons with $\chi_\gamma \gtrsim 1$ are typically emitted.

Within the framework of the doubling chain process model, the number of pairs (multiplicity of the cascade) must grow exponentially,

$$N(t) \sim e^{\Gamma t}, \qquad \Gamma \sim \frac{1}{t_e} \sim \alpha \mu^{1/4} \sqrt{\frac{mc^2 \omega}{\hbar}}. \tag{13}$$

In the next section, we are checking the estimations (12) and (13) by direct Monte-Carlo simulations.

IV. DESCRIPTION OF MONTE-CARLO APPROACH AND NUMERICAL RESULTS

In our simulations we are using a Monte-Carlo approach for the integration of the cascade equations [see the Eqs. (A1) and (A2)]. We trace the motion of the electrons and positrons in between the acts of photon emission classically, whereas for hard photons we exploit the ray tracing approximation in between the acts of their emission and conversion into pairs. Even though there exists the exact analytical solution (8) for equations of motion (7) for positrons and electrons, we are integrating Eq. (7) numerically for each of the particles. This is done in order to incorporate the probabilistic events of photon emission and pair creation in the routines as described below, as well as for the purpose of future generalization to more realistic field configurations.

Our numerical algorithm works as follows. At each time step $t_i < t < t_i + \Delta t$ we are calculating the momenta of all the particles created at the preceding time steps by $\boldsymbol{p}_{i+1} = \boldsymbol{p}_i + q_i \boldsymbol{E}_{i+1/2} \Delta t$, where $\boldsymbol{E}_{i+1/2} = \boldsymbol{E}(t_i + \Delta t/2)$ and $q_i = +e, -e, 0$ for positrons, electrons, and photons, respectively. The event generator determines which of the electrons or positrons is going to emit a photon at this time step and whether any of the present photons is going to produce a pair.

Let us explain our event generator for photon emission in more detail (see also Refs. [22,30]). Starting from $\boldsymbol{p}_i$ and $\boldsymbol{E}_i = \boldsymbol{E}(t_i)$, we attach the value χ_i at time t_i using Eq. (1) to each electron and positron and compute the total probability rate $W_{\rm rad}$. In order to isolate the infrared singularity, we set the lower limit of integration to $\varepsilon_{\rm min}$. For each electron and positron, we assume that it emits a photon between t_i and t_{i+1} if $r < W_{\rm rad}\Delta t$, where r $(0 < r < 1)$ is a uniformly distributed random number. If the above inequality is fulfilled, then the energy ε_γ of the emitted photon is obtained as the root of the sampling equation,

$$\frac{1}{W_{\rm rad}} \int_{\varepsilon_{\rm min}}^{\varepsilon_\gamma} \frac{dW_{\rm rad}(\varepsilon_\gamma)}{d\varepsilon_\gamma} d\varepsilon_\gamma = r', \tag{14}$$

where r' $(0 < r' < 1)$ is an independent random number. The time step Δt, which remains fixed in the course of computation, must be chosen such that the restriction $\Delta t \ll W_{\rm rad}^{-1}, W_{\rm cr}^{-1}$ holds. The direction of propagation of the newly emitted photon is parallel to the momentum $\boldsymbol{p}_i$ of the parental electron or positron, whose momentum after emission we find from the conservation law as discussed in Sec. II. For pair creation, the event generator works similarly, apart from the fact that there is no need for the regularization parameter $\varepsilon_{\rm min}$.

Within the constant crossed field approximation applied here we assume that $\varepsilon_\gamma \gg mc^2$. However, the photons with energies $\varepsilon_\gamma \lesssim mc^2$ are not able to create pairs in a subcritical field, for which $\chi_\gamma \ll 1$. Therefore, we can completely neglect emission of soft photons in our problem. Based on this reasoning, we currently set the lower integration limit $\varepsilon_{\rm min}$ to mc^2 for both $W_{\rm rad}$ and the sampling Eq. (14).

As a benchmark for our code we have simulated the development of a cascade initiated by a high-energy ($\varepsilon_0 = 2 \times 10^5 mc^2$) initial electron in a constant homogeneous transverse field with $E_0 = 0.2 E_S$. Our results are averaged over 10^3 simulation runs. In this particular simulation, the curvature of trajectories of electrons and positrons has been neglected, so that the results of our simulations can be directly compared with previous simulations of cascades produced by high-energy electrons in a magnetic field [24]. Comparison of cascade profiles obtained in both simulations is given in Fig. 3 by the thin black and thick gray lines, respectively. The figure represents the number of pairs with an energy exceeding 0.1% of the energy of the primary electron versus the elapsed time. In our notation the reference characteristic radiation time $t_{\rm rad}$ as adopted in Ref. [24] is $t_{\rm rad} = 3.85 \times (\gamma_{\rm in}/\alpha \chi_{\rm in}^{2/3}) \times (\hbar/mc^2) = 5.64 \times W_{\rm rad,in}^{-1}$, where the subscript "in" refers to the initial

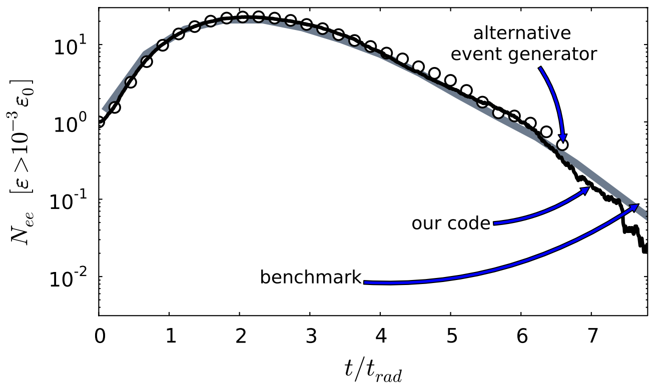

FIG. 3. Comparison of the cascade profile obtained with our code (black thin line), with a code applying an alternative event generator (circles) and from previous independent simulations (thick gray line, see Fig. 5 in [24]). Depicted is the number of pairs with energy $\varepsilon > 10^{-3}\varepsilon_0$ versus the elapsed time. The simulation parameters are $\varepsilon_0 = 100$ GeV and $E_0/E_S = 0.2$.

data for primary electron. We see that our results are in reasonable agreement with the paper [24].

We have also implemented and tested a different event generator, which provides significant speed up due to the absence of numerical integrations. The idea is to exploit some explicit algebraic fits for the energy spectrum (2), and to exchange the order of testing the occurrence of photon emission and of sampling its energy. In this alternative version of the algorithm, within each time step one first samples the possible energy of an emitted photon just as a uniformly distributed random quantity, $\varepsilon_\gamma = \varepsilon_e r'$ in the above notation. After that, photon emission is assumed to take place if $r < [dW_{\rm rad}(\varepsilon_\gamma)/d\varepsilon_\gamma]\varepsilon_e \Delta t$. In this case, the time step must satisfy the condition $\Delta t \ll [\varepsilon_e dW_{\rm rad}(\varepsilon_\gamma^*)/d\varepsilon_\gamma]^{-1}$ for all appearing electrons and positrons, where ε_γ^* is the photon energy that corresponds to the maximum of the emission spectrum (2). The same scheme can be applied to the simulation of pair photoproduction as well. Note that in this case there is no need to introduce the energy cutoff $\varepsilon_{\rm min}$, although this may serve as a useful trick if one wants to restrict the number of soft photons that are traced by the code. The test of the modified event generator is included by circles in Fig. 3. This test demonstrates that both versions of the event generator are in fact equivalent.

The results of our simulations are collected in Figs. 2 and 4–7. Figure 2 represents a typical spatial picture of the formation and development of a cascade initiated by a positron. The electrons and positrons are deflected by the field in opposite directions, whereas the directions of propagation of photons are distributed randomly, as could be expected. For the rest of the paper we assume for all simulations in an uniformly rotating field that at $t = 0$ we have a single electron at rest ($\boldsymbol{p}_e = 0$) and no photons and positrons. The typical evolution of the quantum dynamical parameter χ_e of the primary electron is illustrated with the left panel of Fig. 4. Before the emission of a first photon, the electron is gaining energy and its parameter χ_e is growing as the square of time in accordance with Eq. (10b). After the first photon emission, which for our parameters happens typically on the time scale t_e smaller than ω^{-1}, the curves become stochastic and consist of smooth sections with typical growth of χ_e due to acceleration by the field. These sections are separated by sudden breakdowns resulting from recoils due to successive photon emissions. Since these recoils are random, the three curves in the figure corresponding to independent simulation runs deviate at later times. After the transient period which typically lasts for several lifetimes t_e, the momentum losses due to quantum recoils are coming into equilibrium on the average with the trend of acceleration by the field. After that, function $\chi_e(t)$ for an individual electron describes a stationary stochastic process. This is a

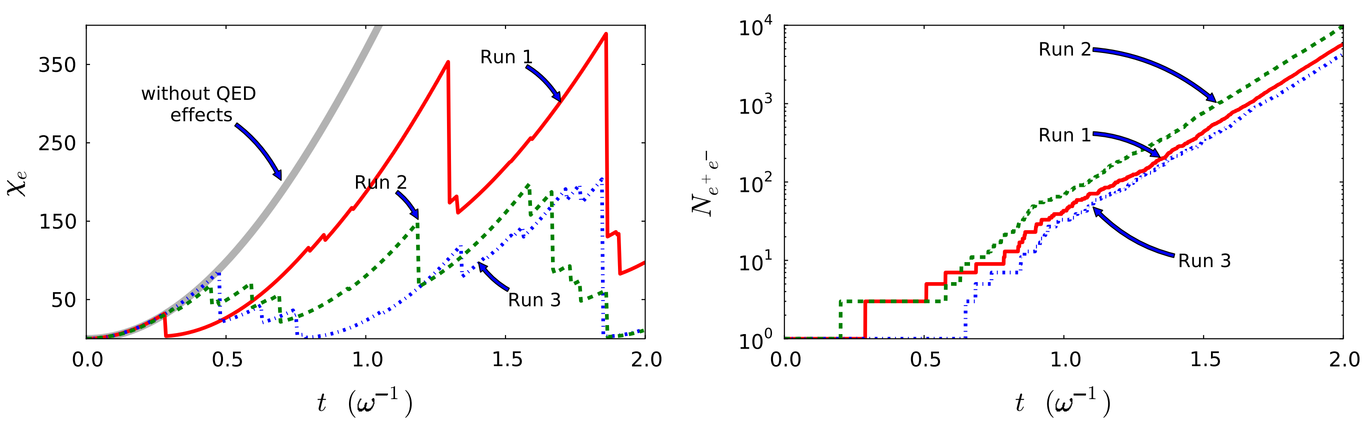

FIG. 4. Left plot: Temporal evolution of the quantum dynamical parameter χ_e of the primary electron for three independent Monte-Carlo simulations. The thick gray curve corresponds to the analytical solution Eq. (9b) for $\chi_e(t)$ in the absence of any QED processes. The three other curves (run 1, run 2, and run 3) are the results of the three independent Monte-Carlo simulations with parameters $a_0 = 2 \times 10^4$ and $\hbar\omega = 1$ eV. Right plot: The total number of electrons and positrons $N_{e^+e^-}$ vs time for the same independent simulations.

manifestation of the restoration mechanism discussed in the preceding section.

As it was predicted in Ref. [10], the development of a cascade results in exponential growth with time of the total numbers of secondary hard photons and electron-positron pairs. This is illustrated with the right panel in Fig. 4. The plot $N_{e^-e^+}(t)$ is given by a random stairway, with each stair corresponding to creation of a single pair. The successive steps are well separated initially, when the total number of pairs remains small. At later time with the number of pairs growing rapidly, the stairlike structure of the lines in the plot becomes invisible and straight lines are obtained. Although these straight lines for independent simulation runs are typically different, mostly because emission of the first photon starts randomly from one simulation run to another, nevertheless their *gradients* are varying weakly in different runs and can be used to determine the growth rate Γ in Eq. (13). For example, the growth rates extracted from the curves 1–3 at Fig. 4 are $\Gamma = 4.62$, 4.84, and 4.90, respectively.

We have studied the averages of the quantities χ_e, ε_e, and θ over the cascade. For example, temporal evolution of the mean value

$$\langle \chi_e(t) \rangle = \frac{1}{N_{e^-}(t)} \sum_{i=1}^{N_{e^-}(t)} \chi_{ei}(t), \qquad (15)$$

where $N_{e^-}(t)$ is the instant number of present electrons and $\chi_{ei}(t)$ is the instant value of the quantum dynamical parameter for the ith electron, is depicted in the left plot of Fig. 5. One can see that at later times the random fluctuations are smoothed out and the quantity (15) stabilizes acquiring some definite constant value which is independent of the simulation run. The same behavior was observed for $\langle \varepsilon_e \rangle$ and $\langle \theta \rangle$, which are defined similarly to Eq. (15). The typical evolution of the averaged energy of all the components of the cascade is represented in the right plot of Fig. 5. At later times, the mean energies of electrons and positrons coincide as is expected from symmetry consideration, whereas the mean photon energy typically remains smaller. At the same time, the energy spectrum of created electrons and positrons is wider than the photon spectrum (see Fig. 6). Both features are explained naturally by the fact that in our setup the hard photons ($\chi_\gamma \gtrsim 1$) are quickly converted into pairs which survive, whereas soft photons ($\chi_\gamma \lesssim 1$) are stable with respect to pair photoproduction and hence are accumulated. In the high energy region, all the spectra are likely to show exponential decay.

One of our main tasks was the investigation of the validity of estimations (12) and (13) which were suggested previously in Ref. [10] and are of crucial importance. In particular, Eq. (13) was serving as an argument for the estimation of the maximum value of the intensity attainable with focused laser fields. In order to test these estimations, we have performed parametric studies of the stabilized values of the quantities $\langle \chi_e \rangle$, $\langle \varepsilon_e \rangle$, $\langle \theta \rangle$ and of the increment Γ. These results are presented in Fig. 7. The ratios $\langle \varepsilon_e \rangle / \varepsilon_{\rm est}$, $\langle \chi_e \rangle / \chi_{\rm est}$, $\langle \theta_e \rangle / \theta_{\rm est}$ as functions of μ are presented in the left plot for the fixed rotation frequency $\hbar\omega = 1$ eV. It is clear from the figure that at large values of μ each ratio acquires some constant value of the order of unity. According to our results the formulas (12) are valid up to some numerical coefficients of the order of unity, which vary no more than twice in the whole range $\mu > 1$. The results of simulations for Γ are compared with Eq. (13) for two different rotation frequencies $\hbar\omega = 0.66$ eV and $\hbar\omega = 1$ eV on the right panel of Fig. 7. One can see that for large values of μ the estimation (13) is justified with good accuracy even without any correction factor. For $\mu \lesssim 30$ formula (13) overestimates Γ but not more than by half of an order of magnitude. This may be nevertheless crucial for the estimation of the total cascade yield due to its exponential dependence on Γ. For the particular value $\mu \approx 10$, which was exploited in Ref. [10], formula (13) overestimates Γ by approximately a factor of 1.5. This, however, is

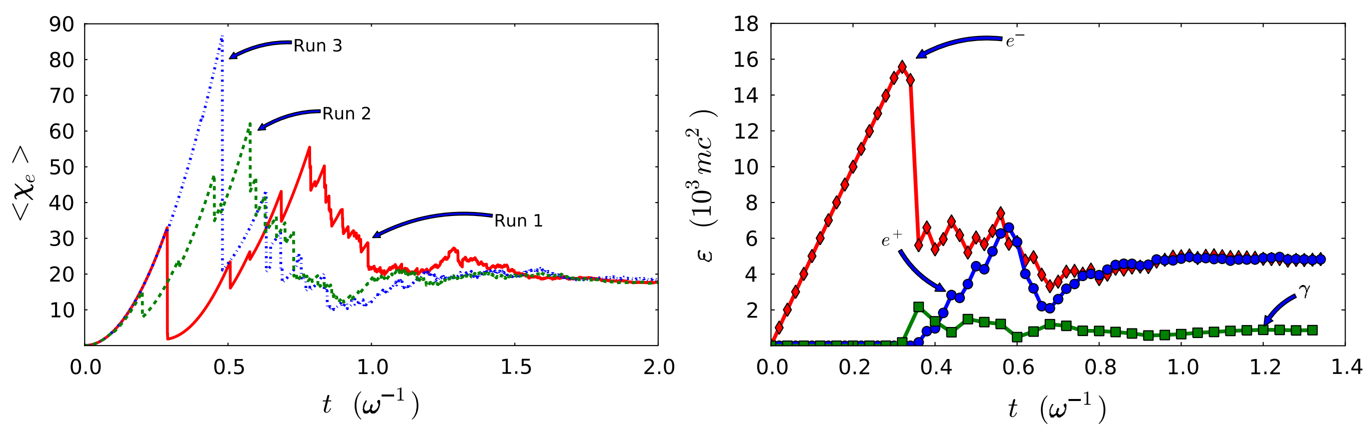

FIG. 5. Left plot: The dynamical quantum parameter $\langle \chi_e \rangle$ for the electrons averaged over the cascade vs time for the same simulations as in Fig. 4. Right plot: Evolution of the mean energy of the electrons, positrons, and photons averaged over the cascade in a typical simulation run ($a_0 = 5 \times 10^4$ and $\hbar\omega = 1$ eV).

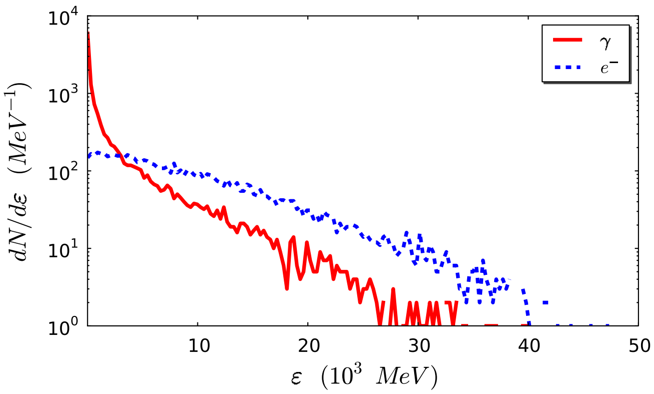

FIG. 6. The energy spectra for different components of the cascade at $t = 1.2 \times \omega^{-1}$ for $a_0 = 5 \times 10^4$ and $\hbar\omega = 1$ eV.

compensated by simultaneous underestimation of the escape time $t_{\rm esc}$ in Ref. [10].

In order to apply the results of our simulations to estimate the cascade yield by a realistic focused laser field, we assume that the appearing electrons and positrons are pushed away as a whole from the focus by the ponderomotive potential in radial direction with almost the speed of light. Assuming the Gaussian profile of the focused beam we can write $\mu(t) = \mu_0 e^{-c^2t^2/w_0^2}$, where μ_0 is the value of the parameter μ at the center of the focus and w_0 is the focal radius. Then the total number of pairs produced by the cascade can be estimated to the

$$\ln(N_{e^+e^-}) \sim \int_0^\infty \Gamma[\mu(t)]dt = \Gamma(\mu_0) \int_0^\infty e^{-c^2t^2/4w_0^2}dt,$$

see Eq. (13). The remaining integral defines the effective time of escape from the focus and equals $\sqrt{\pi}(w_0/c)$, i.e., is $\sqrt{\pi} \approx 1.77$ times larger than it was assumed in Ref. [10]. This correction almost totally cancels the overestimation of Γ by formula (13) at $\mu \approx 10$ that we have observed in our simulations. Thus, we hope that the quantitative predictions in Ref. [10] must remain unaffected by our corrections.

One can see that we are currently neglecting the complicating details in our code such as elastic collisions, Compton scattering, and annihilation processes. Such phenomena must become important only at longer time scales, when the plasma is dense enough. Though successive collisions and annihilations of the electron and positron from the same created pair may be important [31], we are currently ignoring these effects for simplicity [32]. We ignore the higher-order processes, such as two-photon creation and the trident processes as well (see the remark at the end of Sec. II). All these assumptions are natural and commonly accepted in the present cascade theory [23], even though they may be revised in future studies.

Because of limitations of computer power, we currently stop our simulations after the creation of $N_{e^-e^+} \lesssim 10^4$ pairs. This was shown to be enough to estimate the growth rate Γ, as well as to average the characteristics of a cascade over the ensemble of pairs with reasonable accuracy. In the time interval of simulation these pairs occupy a volume of the order d^3, where $d \sim c/\omega \sim 1$ μm. This corresponds to a pair density $n_{e^+e^-} \sim 10^{16}$ cm^{-3}. Typical values of the γ factor for electrons and positrons are $\gamma \sim 10^3$–10^4 (see Fig. 6), corresponding to energies $\varepsilon_e = \gamma mc^2 \sim$ 0.5–5 GeV. Assuming a temperature $T \sim \varepsilon_e/k \sim 10^{13}$ K, we can estimate the Debye screening radius $r_D \sim \sqrt{kT/e^2n_{e^+e^-}} \sim 1$ cm $\gg d$. The relativistic plasma frequency $\Omega_{\rm pe} \sim c/r_D \sim 10^{10}$ sec^{-1} remains about 5 orders of magnitude smaller than the optical frequency. For these reasons we have completely neglected Coulomb interaction between electrons and positrons and all the accompanying collective plasma effects in the present simulations.

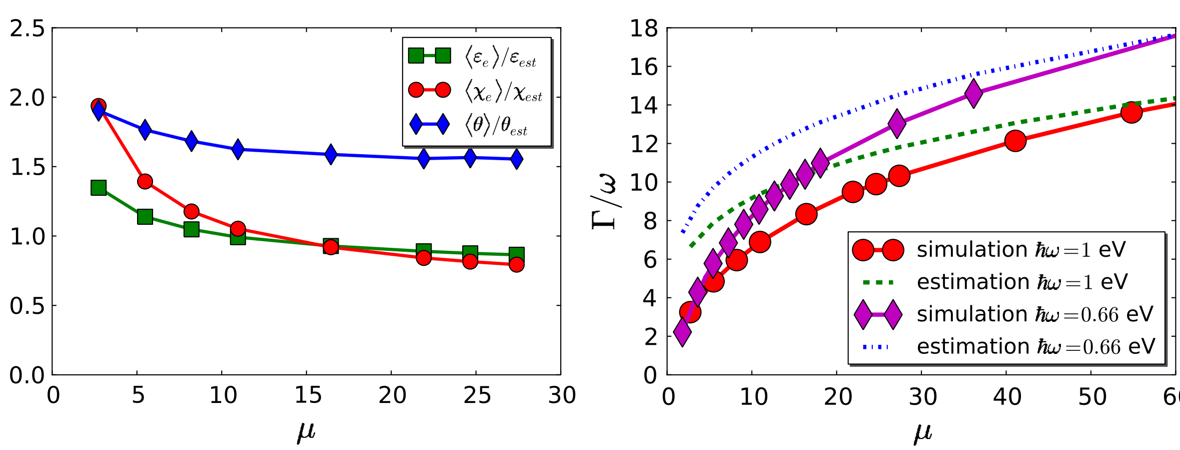

FIG. 7. Left plot: Parametric studies of the mean energy $\langle\varepsilon_e\rangle$, the mean dynamical quantum parameter $\langle\chi_e\rangle$, and the mean angle $\langle\theta\rangle$ between the momentum and the field for electrons and positrons. The ratios of the simulation results to the approximations (12b) and (12c), are plotted vs the parameter μ for $\hbar\omega = 1$ eV. Right plot: Parametric study of the increment Γ as a function of the dimensionless field strength μ for two rotation frequencies $\hbar\omega = 1$ eV and $\hbar\omega = 0.66$ eV. The approximation (13) is shown by the dashed lines.

However, the density of pairs is growing exponentially, $n_{e^+e^-}(t) \propto e^{\Gamma t}$, and hence $r_D \propto e^{-\Gamma t/2}$ and $\Omega_{\rm pe} \propto e^{\Gamma t/2}$. After a relatively short period of time $\lesssim 2\pi/\omega$, when the number of pairs becomes macroscopic ($\sim 10^{11}$), the quantities r_D and $\Omega_{\rm pe}$ attain the values d and ω, respectively, and the collective plasma effects may come into play. Within our approximation of a homogeneous field, the total number of created pairs would be restricted by the screening of the external field by the self-field of arising plasma.

Let us note that, despite some doubts expressed in [25], the radiation friction is taken into account properly in our version of the algorithm by the recoils happening at the times of photon emission (see, e.g., Ref. [33] and the Appendix in our paper). Hence, there is no need to include an additional radiation friction force in the equations of motion (7) for electrons and positrons as this would cause double counting. Moreover, our approach transfers the concept of classical radiation friction into the quantum domain in a correct fashion. It can be asked how the classical continuously acting radiation friction can be recovered from the sudden jumps of momentum similar to those in Fig. 4. In fact this happens on the average with respect to the ensemble of Monte-Carlo realizations, since the moments of successive photon emissions are distributed randomly. At a longer time, when the number of created pairs becomes large, the cascade forms a representative ensemble itself, and there is in principle no need for averaging over independent realizations.

V. SUMMARY AND DISCUSSION

In this paper we have presented the first results of numerical simulations of the formation and development of electron-positron-photon cascades by initially slow electrons in a uniformly rotating homogeneous electric field. In such a situation the cascades reveal a new feature, i.e., the restoration of the energy and the dynamical quantum parameter due to the acceleration of electrons and positrons by the field. This feature may be of crucial importance for the physics of laser-matter interactions in the strong field domain, as it was demonstrated in Ref. [10]. We have explicitly identified this restoration mechanism in the course of our simulations. Also, our simulations clearly confirm the qualitative analysis of Ref. [10], including the basic scaling relations (12) and the estimate (13) for the cascade yield. So, they can be used to fix the remaining numerical prefactors in Eqs. (12) and (13) (which turn out to be of the order of unity).

The numerical approach that we adopt is based on Monte-Carlo simulations of the cascade equations. We have shown explicitly that contrary to some doubts expressed in the literature [25] such an approach incorporates radiation friction acting on individual electrons and positrons and, moreover, is doing this in a manner which is consistent with intense field QED.

The code designed for our task can be readily adopted for simulating cascades in the laser fields with more realistic configurations, such as tightly focused Gaussian beams and pulses. This is required in order to make more definite predictions on the impact of cascade production for possible future experiments, as well as for further corrections of the maximum value of intensity that can be attained with optical lasers [10]. A simulation of cascades in a focused laser field will be presented in a separate publication. However, let us make several brief comments about cascades in focused laser fields, possible experimental scenarios, and some yet unresolved technical problems that may require further studies.

The restoration mechanism arises due to the curvature of the trajectories of the charged particles across the field and may be sensitive to its polarization. Although we expect that this mechanism must work for generic field configurations (e.g., for generic tightly focused laser fields), there may exist several particular configurations for which the restoration mechanism does not work. For example, in an arbitrary constant electromagnetic field or a circularly polarized propagating plane electromagnetic wave, the dynamical quantum parameter χ_e is conserved exactly in the course of motion. In the case of a generic propagating plane wave the amplitude of oscillations of the parameter χ_e for an initially slow electron does not exceed E_0/E_S, i.e., always remains smaller than unity. Another example is a linearly polarized oscillating electric field [25], since in this case the initially slow particles are accelerated strictly along the field and hence the growth of the transverse component of the field is absent. In some intermediate cases, e.g., for elliptical polarization or a weakly focused Gaussian beam, restoration of χ_e must exist but may be less effective than in the case of circular polarization. However, in all cases at least the usual cascades would be caused by external high-energy electrons or hard photons passing through the high-field region transverse to the field. This means that the cascade yield remains microscopic and would be determined by both the initial energy of an external energetic particle and the laser field strength.

In order to initiate a cascade in a tightly focused laser field, one needs to inject a primary particle into the center of a focal region. This task may be nontrivial because the focal region is surrounded by a ponderomotive potential wall of the characteristic height $U_0 \sim mc^2\sqrt{1+a_0^2} \approx mc^2 a_0$. The external high-energy electrons will most likely not penetrate inside, but rather will be deflected. The most direct and elegant scenario is based on the exploration of pairs that are created spontaneously from vacuum by the laser field itself [10], since they are appearing exactly at the center of the focus as required. However, this possibility implies high intensities $\gtrsim 10^{26}\ \mathrm{W/cm^2}$. Another possible resolution would be the initiation of cascades by energetic γ quanta. In our opinion, the ultimate question of whether or not cascades *with macroscopic yield* can arise in *generic* real experiments exploring laser-matter interaction at intensities lower than $\sim 10^{26}$ W/cm^2 requires further studies. We note that for cascades that arise in the course of the interaction of high-intensity laser radiation with material targets it may be necessary to take into account the impact of ordinary cascades in matter as well [34].

If the cascade yield attains macroscopic values ($N_{e^-e^+} \sim 10^{11}$), the self-field of the electron-positron plasma becomes comparable to the guiding field. In this regime screening of the external field and its absorption by the electron-positron plasma self-field will restrict further pair production. Such a regime can be simulated by combining our code with the particle-in-cell (PIC) method [35]. We hope to address this problem in the near future.

ACKNOWLEDGMENTS

We are grateful to G. Korn for his permanent interest in this work and useful advise. We are also grateful to S. V. Bulanov, J. Kirk, A. Bell, and I. Sokolov for fruitful disputes that gave us several useful ideas and to E. Vilenius and S. Rykovanov for reading this manuscript and suggesting a number of stylistic corrections. This work was supported by the Grant No. DFG RU 633/1-1, the Cluster-of-Excellence "Munich-Centre for Advanced Photonics" (MAP), the Dynasty foundation, Russian Fund for Basic Research, the Ministry of Science and Education of the Russian Federation and the Russian Federal Program "Scientific and scientific-pedagogical personnel of innovative Russia".

APPENDIX: CASCADE EQUATIONS AND RADIATION REACTION

The cascade equations for a uniformly rotating homogeneous electric field,

$$\begin{aligned} &\frac{\partial f_\pm(\boldsymbol{p}_e, t)}{\partial t} \pm e\boldsymbol{E}(t)\frac{\partial f_\pm(\boldsymbol{p}_e, t)}{\partial \boldsymbol{p}_e} \\ &= \int w_{\rm rad}(\boldsymbol{p}_e + \boldsymbol{p}_\gamma \to \boldsymbol{p}_\gamma) f_\pm(\boldsymbol{p}_e + \boldsymbol{p}_\gamma, t) d^3 p_\gamma \\ &\quad - f_\pm(\boldsymbol{p}_e, t)\int w_{\rm rad}(\boldsymbol{p}_e \to \boldsymbol{p}_\gamma) d^3 p_\gamma \\ &\quad + \int w_{\rm cr}(\boldsymbol{p}_\gamma \to \boldsymbol{p}_e) f_\gamma(\boldsymbol{p}_\gamma, t) d^3 p_\gamma, \end{aligned} \tag{A1}$$

$$\begin{aligned} \frac{\partial f_\gamma(\boldsymbol{p}_\gamma, t)}{\partial t} &= \int w_{\rm rad}(\boldsymbol{p}_e \to \boldsymbol{p}_\gamma)[f_+(\boldsymbol{p}_e, t) + f_-(\boldsymbol{p}_e, t)] d^3 p_e \\ &\quad - f_\gamma(\boldsymbol{p}_\gamma, t)\int w_{\rm cr}(\boldsymbol{p}_\gamma \to \boldsymbol{p}_e) d^3 p_e, \end{aligned} \tag{A2}$$

differ from the standard equations of EAS [12,13] only by addition of the second term to the left-hand side of Eq. (A1), which takes into account electron and positron acceleration. Here, $f_\pm$ and f_γ are the distribution functions for positrons, electrons, and photons, respectively. In our approximation the momenta of emitted photon, as well as of created electron and positron, are directed strictly along the direction of motion of the parental particle. This means that the differential probability rates can be written in the form

$$\begin{aligned} w_{\rm rad}(\boldsymbol{p}_e \to \boldsymbol{p}_\gamma) &= \int_0^1 d\lambda\, \delta(\boldsymbol{p}_\gamma - \lambda \boldsymbol{p}_e)\epsilon_e \frac{dW_{\rm rad}}{d\varepsilon_\gamma}\bigg|_{\varepsilon_\gamma = \lambda\varepsilon_e}, \\ w_{\rm cr}(\boldsymbol{p}_\gamma \to \boldsymbol{p}_e) &= \int_0^1 d\lambda\, \delta(\boldsymbol{p}_e - \lambda \boldsymbol{p}_\gamma)\epsilon_\gamma \frac{dW_{\rm cr}}{d\varepsilon_e}\bigg|_{\varepsilon_e = \lambda\varepsilon_\gamma}, \end{aligned} \tag{A3}$$

so that the threefold integrals on the right-hand side (RHS) of Eqs. (A1) and (A2) transform into onefold integrals. However, the problem does not become one dimensional since the direction of the field $\boldsymbol{E}(t)$ varies in time.

It is worth noting that owing to Eq. (A3) it follows from (A1) and (A2) that

$$\begin{aligned} &\frac{d}{dt}\left\{\int \boldsymbol{p}_e(f_+ + f_-)d^3 p_e + \int \boldsymbol{p}_\gamma f_\gamma d^3 p_\gamma\right\} \\ &\quad = e\boldsymbol{E}(t)\int (f_+ - f_-) d^3 p_e, \end{aligned} \tag{A4}$$

$$\begin{aligned} &\frac{d}{dt}\left\{\int \varepsilon_e(f_+ + f_-)d^3 p_e + \int \varepsilon_\gamma f_\gamma d^3 p_\gamma\right\} \\ &\quad = e\boldsymbol{E}(t)\int \frac{\boldsymbol{p}_e}{\varepsilon_e}(f_+ - f_-) d^3 p_e. \end{aligned} \tag{A5}$$

These relations demonstrate that in our approximation the momentum and the energy of particles are derived from the field only in the process of acceleration of electrons and positrons. By turn, this means that the energy and the momentum of the electron-positron-photon plasma are conserved in events of photon emission and pair photoproduction.

The first two terms on the RHS of Eq. (A1) describe the influence of photon emission on the motion of electrons and positrons. Let us demonstrate that the classical radiation reaction is taken into account by these terms properly. For this purpose we will consider the domain of $\chi_{e\pm} \ll 1$ (at the same time the particles are assumed to be ultrarelativistic as before). In this case the motion of the particles can be considered completely classical. Then the third term on the RHS of Eq. (A1), which is responsible for pair production, can be omitted and, hence, the total numbers of positrons and electrons $N_\pm = \int f_\pm d^3 p_e$ are conserved.

Let us rewrite the relation between the variables χ_γ and x in Eq. (2) in the form

$$\chi_\gamma = \frac{x^{3/2}\chi_e^2}{1 + x^{3/2}\chi_e}. \tag{A6}$$

Taking into account that the spectrum (2) of the emitted photons is effectively concentrated in the range $x \lesssim 1$, we get

$$\chi_\gamma \approx x^{3/2}\chi_e^2 \lesssim \chi_e^2 \ll \chi_e. \tag{A7}$$

As a consequence, $p_\gamma \ll p_e$ and in the remaining integrals on the RHS of Eq. (A1) we can use the expansion

$$w_{\rm rad}(\boldsymbol{p}_e + \boldsymbol{p}_\gamma \to \boldsymbol{p}_\gamma) f_\pm(\boldsymbol{p}_e + \boldsymbol{p}_\gamma) - w_{\rm rad}(\boldsymbol{p}_e \to \boldsymbol{p}_\gamma) f_\pm(\boldsymbol{p}_e) \approx \boldsymbol{p}_\gamma \frac{\partial}{\partial \boldsymbol{p}_e}[w_{\rm rad}(\boldsymbol{p}_e \to \boldsymbol{p}_\gamma) f_\pm(\boldsymbol{p}_e)]. \tag{A8}$$

Now, we multiply both sides of the transformed Eq. (A1) by $\boldsymbol{p}_e$ and integrate it over $\boldsymbol{p}_e$. The result can be easily reduced to the form

$$\dot{\boldsymbol{P}}_\pm(t) = \pm e\boldsymbol{E}(t) + \langle \boldsymbol{R} \rangle_\pm(t), \tag{A9}$$

where $\boldsymbol{P}_\pm(t) = (1/N_\pm)\int \boldsymbol{p}_e f_\pm(\boldsymbol{p}_e, t) d^3 p_e$ are the average momenta of positrons and electrons,

$$\boldsymbol{R}(\boldsymbol{p}_e) = -\int \boldsymbol{p}_\gamma w_{\rm rad}(\boldsymbol{p}_e \to \boldsymbol{p}_\gamma) d^3 p_\gamma \tag{A10}$$

is the mean rate of momentum losses of the particles due to photon emission, and

$$\langle \boldsymbol{R} \rangle_\pm(t) = \frac{1}{N_\pm}\int \boldsymbol{R}(\boldsymbol{p}_e) f_\pm(\boldsymbol{p}_e, t) d^3 p_e$$

are its mean values.

Taking into account that $\boldsymbol{p}_\gamma \approx x^{3/2}\chi_e \boldsymbol{p}_e$ and $\varepsilon_\gamma = (\varepsilon_e/\chi_e)\chi_\gamma$ and using Eqs. (A3) and (2), we obtain

$$\boldsymbol{R}(\boldsymbol{p}_e) = -\varepsilon_e \boldsymbol{p}_e \int_0^{\chi_e} x^{3/2} \frac{dW_{\rm rad}}{d\varepsilon_\gamma} d\chi_\gamma. \tag{A11}$$

From this point, we pass to the integration over the variable x. In the approximation $\chi_e \ll 1$ we have $\chi_\gamma = x^{3/2}\chi_e^2$. The main contribution to the integral in Eq. (A11) comes from the range $x \sim 1$. Hence, we can neglect the term $\chi_\gamma\sqrt{x}$ in the brackets on the RHS of Eq. (2) and, in addition, replace the upper limit of integration over x by infinity. After these manipulations, we have

$$\boldsymbol{R} = \frac{3}{2}\frac{\alpha m^2 c^4 \chi_e^2}{\hbar}\frac{\boldsymbol{p}_e}{\varepsilon_e} J, \qquad J = \int_0^\infty \left\{ x^2 \int_x^\infty {\rm Ai}(\xi) d\xi + 2x{\rm Ai}'(x) \right\} dx. \tag{A12}$$

The remaining integral J after integration by parts and use of the Airy equation, ${\rm Ai}''(x) - x{\rm Ai}(x) = 0$, is reduced to

$$J = -\frac{2}{3}\int_0^\infty x^3 {\rm Ai}(x) dx = -\frac{4}{9}.$$

Thus, in view of Eq. (1), we finally have

$$\boldsymbol{R} = -\frac{2}{3}\frac{\alpha m^2 c^4 \chi_e^2}{\hbar}\frac{\boldsymbol{p}_e}{\varepsilon_e} = -\frac{2}{3}\frac{e^4 F_\perp^2 \gamma_e^2}{m^2 c^4}\frac{c\boldsymbol{p}_e}{\varepsilon_e}. \tag{A13}$$

This is exactly the leading term of the Landau-Lifshitz (LL) force for ultrarelativistic electrons [26]. Other terms of the LL force do not appear in (A13) only because we have used the approximation of ultrarelativistic particles in our derivation from the very beginning.

In the quantum case $\chi_e \gg 1$ the expansion (A8) is not valid. Thus, radiation friction in the quantum regime cannot be described by the concept of classical force in principle, as it was attempted to do, e.g., in [9]. In addition to the advection term in the transport equation, which could be ascribed to the radiation reaction force as above, spreading of the distribution functions in momentum space becomes important as well. This spreading is associated with quantum fluctuations and is observable, e.g., as quantum excitation of synchrotron and betatron oscillations [36].

[1] G. A. Mourou *et al.*, Rev. Mod. Phys. **78**, 309 (2006); M. Marklund and P. Shukla, Rev. Mod. Phys. **78**, 591 (2006); Y. I. Salamin *et al.*, Phys. Rep. **427**, 41 (2006); T. Heinzl and A. Ilderton, Eur. Phys. J. D **55**, 359 (2009).
[2] V. Yanovsky *et al.*, Opt. Express **16**, 2109 (2008).
[3] M. Dunne, Nature Phys. **2**, 2 (2006).
[4] *Extreme Light Infrastructure: Report on the Grand Challenges Meeting*, edited by G. Korn and P. Antici (ELI/Ecole Polytechnique, Paris, 2009), http://www.eli-laser.eu/reports.php.
[5] T. Tajima and G. Mourou, Phys. Rev. ST Accel. Beams **5**, 031301 (2002).
[6] S. V. Bulanov, T. Esirkepov, and T. Tajima, Phys. Rev. Lett. **91**, 085001 (2003); A. S. Pirozhkov *et al.*, Phys. Plasmas **14**, 123106 (2007).
[7] S. Gordienko, A. Pukhov, O. Shorokhov, and T. Baeva, Phys. Rev. Lett. **94**, 103903 (2005).
[8] A. R. Bell and J. G. Kirk, Phys. Rev. Lett. **101**, 200403 (2008).
[9] J. G. Kirk, A. R. Bell, and I. Arka, Plasma Phys. Controlled Fusion **51**, 085008 (2009).
[10] A. M. Fedotov, N. B. Narozhny, G. Mourou, and G. Korn, Phys. Rev. Lett. **105**, 080402 (2010).
[11] P. Auger *et al.*, Rev. Mod. Phys. **11**, 288 (1939).
[12] T. K. Gaisser, *Cosmic Rays and Particle Physics* (Cambridge University Press, New York, 1990).
[13] A. T. Bharucha-Reid, *Elements of the Theory of Markov Processes and Their Applications* (McGraw-Hill, New York, 1960).
[14] H. R. Reiss, J. Math. Phys. (N.Y.) **3**, 59 (1962).
[15] A. I. Nikishov and V. I. Ritus, Sov. Phys. JETP **19**, 529 (1964); **25**, 1135 (1967).
[16] L. S. Brown and T. W. B. Kibble, Phys. Rev. **133**, A705 (1964).
[17] I. I. Gol'dman, Sov. Phys. JETP **19**, 954 (1964); Phys. Lett. **8**, 103 (1964).
[18] T. Erber, Rev. Mod. Phys. **38**, 626 (1966).
[19] V. N. Baier and V. M. Katkov, Phys. Lett. A **25**, 492 (1967).
[20] C. Bamber *et al.*, Phys. Rev. D **60**, 092004 (1999).
[21] V. V. Usov and D. B. Melrose, Aust. J. Phys. **48**, 571 (1995); A. N. Timokhin, arXiv:0912.5475.
[22] J. C. Butcher and H. Messel, Phys. Rev. **112**, 2096 (1958).
[23] A. I. Akhiezer, N. P. Merenkov, and A. P. Rekalo, J. Phys. G **20**, 1499 (1994).

[24] V. Anguelov and H. Vankov, J. Phys. G **25**, 1755 (1999).
[25] S. S. Bulanov *et al.*, Phys. Rev. Lett. **105**, 220407 (2010).
[26] L. D. Landau and I. M. Lifshitz, *Theoretical Physics: The Classical Theory of Fields*, Vol. 2, Course of Theoretical Physics Series (Pergamon Press, London, 1988).
[27] E. M. Lifshitz, L. P. Pitaevskii, and V. B. Berestetskii, *Landau-Lifshitz Course of Theoretical Physics, Quantum Electrodynamics* (Reed Educational and Professional Publishing, Oxford, 1982), Vol. 4.
[28] F. Bloch and A. Nordsiek, Phys. Rev. **52**, 54 (1937); R. J. Glauber, Phys. Rev. **84**, 395 (1951); P. P. Kulish and L. D. Faddeev, Teor. Mat. Fiz. **4**, 153 (1970) [Theor. Math. Phys. **4**, 745 (1970)].
[29] This conservation law is satisfied exactly in a globally constant crossed field.
[30] I. V. Sokolov *et al.*, Phys. Rev. E **81**, 036412 (2010).
[31] M. Yu. Kuchiev, Phys. Rev. Lett. **99**, 130404 (2007).
[32] Note in addition that the arguments of the paper [31] may be irrelevant to our domain of parameters, because the time of recollisions essentially exceeds the time $\sim t_e$ of hard photon emission which destroys the spatial coherence of field-driven oscillations of electron and positron.
[33] A. Di Piazza, K. Z. Hatsagortsyan, and C. H. Keitel, Phys. Rev. Lett. **105**, 220403 (2010).
[34] E. P. Liang, S. C. Wilks, and M. Tabak, Phys. Rev. Lett. **81**, 4887 (1998).
[35] C. K. Birdsall and A. B. Langdon, *Plasma Physics via Computer Simulation* (McGraw-Hill, New York, 1985); J. M. Dawson, Rev. Mod. Phys. **55**, 403 (1983).
[36] A. A. Sokolov and I. M. Ternov, *Synchrotron Radiation* (Pergamon, Berlin, 1968).